Deterministic Entanglement of Two Trapped Ions

Q. A. Turchette,* C. S. Wood, B. E. King, C. J. Myatt, D. Leibfried,† W. M. Itano, C. Monroe, and D. J. Wineland

Time and Frequency Division, National Institute of Standards and Technology, Boulder, Colorado 80303

We have prepared the internal states of two trapped ions in both the Bell-like singlet and triplet entangled states. In contrast to all other experiments with entangled states of either massive particles or photons, we do this in a deterministic fashion, producing entangled states *on demand* without selection. The deterministic production of entangled states is a crucial prerequisite for large-scale quantum computation. [S0031-9007(98)07411-0]

Since the seminal discussions of Einstein, Podolsky, and Rosen, two-particle quantum entanglement has been used to magnify and confirm the peculiarities of quantum mechanics [1]. More recently, quantum entanglement has been shown to be not purely of pedagogical interest, but also relevant to computation [2], information transfer [3], cryptography [4], and spectroscopy [5,6]. Quantum computation (QC) exploits the inherent parallelism of quantum superposition and entanglement to perform certain tasks more efficiently than can be achieved classically [7].

Relatively few physical systems are able to approach the severe requirements of QC: Controllable coherent interaction between the quantum information carriers (quantum bits or qubits), isolation from the environment, and high-efficiency interrogation of individual qubits. Cirac and Zoller have proposed a *scalable* scheme utilizing trapped ions for QC [8]. In it, the qubits are two internal states of an ion; entanglement and computation are achieved by quantum logic operations on pairs of ions involving shared quantized motion. Previously, trapped-ion quantum logic operations were demonstrated between a single ion's motion and its spin [9]. In this Letter, we use conditional quantum logic transformations to entangle and manipulate the qubits of two trapped ions.

Previous experiments have studied entangled states of photons [10,11] and of massive particles [12–14]. These experiments rely on *random processes,* either in creation of the entanglement in photon cascades [10], photon down-conversion [11], and proton scattering [12], or in the selection of appropriate atom pairs from a larger sample of trials in cavity QED [13]. Recent results in NMR of bulk samples have shown entanglement of particle spins [14,15], but because pseudopure states are selected through averaging over a thermal distribution, the signal is exponentially degraded as the number of qubits is increased. In the preceding experiments the efficiency of state generation will exponentially decrease with the system size (both particles and operations). This is because the preceding processes are *selectable* but not *deterministic* generators of entanglement. We mean deterministic as defined in Ref. [16] which in the present context is "the property that if the [entanglement] source

is switched on, then with a high degree of certainty [the desired quantum state of all of a given set of particles is generated] at a known, user-specified time." Deterministic entanglement coupled with the ability to store entangled states for future use is crucial for the realization of large-scale quantum computation. Ion-trap QC has no fundamental scaling limits; moreover, even the simple two-ion manipulations described here can, in principle, be incorporated into large-scale computing by coupling two-ion subsystems via cavities [17], or by using accumulators [6].

In this Letter, we describe the deterministic generation of a state which under ideal conditions is given by

$$|\psi_e(\phi)\rangle = \tfrac{3}{5}|\downarrow\uparrow\rangle - e^{i\phi}\tfrac{4}{5}|\uparrow\downarrow\rangle, \qquad (1)$$

where $|\downarrow\rangle$ and $|\uparrow\rangle$ refer to internal electronic states of each ion (in the usual spin-$1/2$ analogy) and ϕ is a controllable phase factor. For $\phi = 0$ or π, $|\psi_e(\phi)\rangle$ is a good approximation to the usual Bell singlet $(-)$ or triplet $(+)$ state $|\psi_B^\mp\rangle = [|\downarrow\uparrow\rangle \mp |\uparrow\downarrow\rangle]/\sqrt{2}$ since $|\langle\psi_B^-|\psi_e(0)\rangle|^2 = |\langle\psi_B^+|\psi_e(\pi)\rangle|^2 = 0.98$ and $E[\psi_e(\phi)] = 0.94$ where E is the *entanglement* defined in [18]. We also describe a novel means of differentially addressing each ion to generate the entanglement and a state-sensitive detection process to characterize it, leading to a measured fidelity of our experimentally generated state described by density matrix $\rho^\pm$ of $\langle\psi_e(\pi,0)|\rho^\pm|\psi_e(\pi,0)\rangle \approx \langle\psi_B^\pm|\rho^\pm|\psi_B^\pm\rangle \approx 0.70$.

The apparatus is described in Ref. [19]. We confine $^9\mathrm{Be}^+$ ions in an elliptical rf Paul trap (major axis ≈ 525 μm, aspect ratio 3:2) with a potential applied between ring and end caps of $V_0 \cos\Omega_T t + U_0$ with $\Omega_T/2\pi \approx 238$ MHz, $V_0 \approx 520$ V. The trap is typically operated over the range $12 < U_0 < 17$ V leading to secular frequencies of $(\omega_x, \omega_y, \omega_z)/2\pi = (7.3, 16, 12.6)$ to $(8.2, 17.2, 10.1)$ MHz. The ion-ion spacing (along $\hat{x}$) is $l \approx 2$ μm.

The relevant level structure of $^9\mathrm{Be}^+$ is shown in Fig. 1a. The qubit states are the $2s\,{}^2S_{1/2}\,|F = 2, m_F = 2\rangle \equiv |\downarrow\rangle$ and $2s\,{}^2S_{1/2}\,|F = 1, m_F = 1\rangle \equiv |\uparrow\rangle$ states. Laser beams D1 and D2 provide Doppler precooling and beam D3 prevents optical pumping to the $|F = 2, m_F = 1\rangle$ state. The cycling $|\downarrow\rangle \to 2p\,{}^2P_{3/2}$

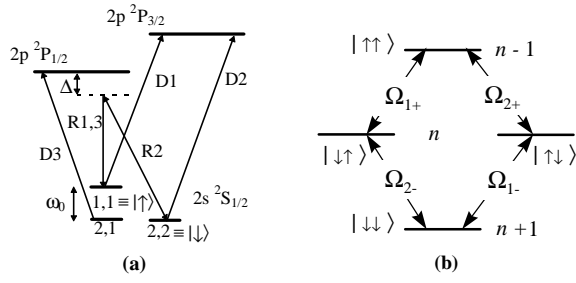FIG. 1. (a) Relevant ^{9}Be$^+$ energy levels. All optical transitions are near $\lambda = 313$ nm, $\Delta/2\pi = 40$ GHz, and $\omega_0/2\pi = 1.25$ GHz. R1–R3: Raman beams. D1–D3: Doppler cooling, optical pumping, and detection beams. (b) The internal basis qubit states of two spins shown with the vibrational levels connected on the red motional sideband. The labeled atomic states are as in (a); n is the motional-state quantum number (note that the motional mode frequency $\omega_{\text{str}} \ll \omega_0$). $\Omega_{i\pm}$ are the Rabi frequencies connecting the states indicated.

$|F = 3, m_F = 3\rangle$ transition driven by the σ^+-polarized D2 laser beam allows us to differentiate $|\uparrow\rangle$ from $|\downarrow\rangle$ in a single ion with $\approx 90\%$ detection efficiency by observing the fluorescence.

Transitions $|\downarrow\rangle|n\rangle \leftrightarrow |\uparrow\rangle|n'\rangle$ (where n, n' are vibrational quantum numbers) are driven by stimulated Raman processes from pairs of laser beams in one of two geometries. Additionally, two types of transitions are driven: the "carrier" with $n' = n$, and the red motional sideband (rsb) with $n' = n - 1$ [20]. With reference to Fig. 1a, the pair of Raman beams R1⊥R2 has difference wave vector $\delta\vec{k} \parallel \hat{x}$ and is used for sideband cooling (to prepare $|\downarrow\downarrow\rangle|0\rangle$), driving the $\hat{x}$ rsb, and to drive the "$\hat{x}$ carrier." Beam pair R2 $\parallel$ R3 with $\delta\vec{k} \approx 0$ drives the "copropagating carrier" and is insensitive to motion.

Two trapped ions aligned along $\hat{x}$ have two modes of motion along $\hat{x}$: the center-of-mass (c.m.) mode (at ω_x) and the stretch mode (at $\omega_{\text{str}} = \sqrt{3}\,\omega_x$) in which the two ions move in opposite directions. We sideband cool both of these modes to near the ground state, but use the stretch mode on transitions which involve the motion since it is colder (99% probability of $|n = 0\rangle$)
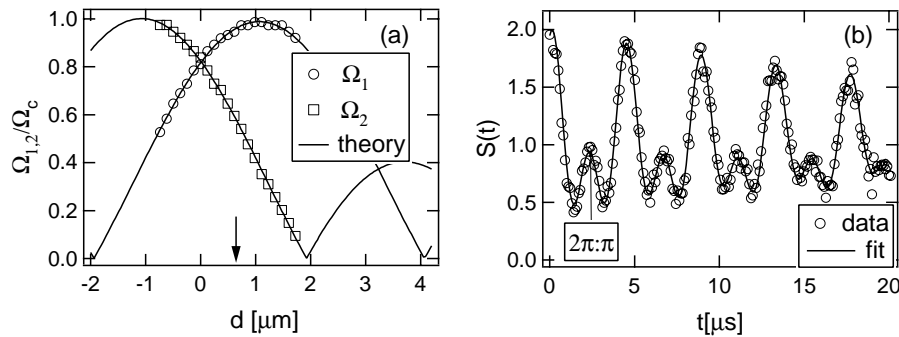
than the c.m. and heats at a significantly reduced rate [19]. Figure 1b shows the relevant states coupled on the rsb with Rabi frequencies (in the Lamb-Dicke limit)

$$\Omega_{i+} = \sqrt{n}\,\eta'\Omega_i; \qquad \Omega_{i-} = \sqrt{n+1}\,\eta'\Omega_i, \quad (2)$$

where $\eta' = \eta/\sqrt{2\sqrt{3}}$ is the stretch-mode two-ion Lamb-Dicke parameter (with single-ion $\eta \approx 0.23$ for $\omega_x/2\pi \approx 8$ MHz) and Ω_i is the carrier Rabi frequency of ion i [9]. On the carrier the time evolution is simply that of independent Rabi oscillations with Rabi frequencies Ω_i. On the copropagating carrier, $\Omega_1 = \Omega_2 \equiv \Omega_c$.

In the Cirac-Zoller scheme, each of an array of tightly focused laser beams illuminates one and only one ion for individual state preparation. Here, each ion is equally illuminated, and we pursue an alternative technique to attain $\Omega_1 \neq \Omega_2$. Differential Rabi frequencies can be used conveniently for individual addressing on the $\hat{x}$ carrier: for example, if $\Omega_1 = 2\Omega_2$, then ion 1 can be driven for a time $\Omega_1 t = \pi$ (2π pulse, no spin flip) while ion 2 is driven for a π pulse resulting in a spin flip.

For differential addressing, we control the ion micromotion. To a good approximation, we can write [21]

$$\Omega_i = \Omega_c J_0(|\delta\vec{k}|\xi_i), \quad (3)$$

where J_0 is the zero-order Bessel function and ξ_i is the amplitude of micromotion at Ω_T (along $\hat{x}$) associated with ion i, proportional to the ion's mean $\hat{x}$ displacement from trap center. The Bessel function arises because the micromotion effectively smears out the position of an ion, thereby suppressing the laser-atom interaction [21]. The micromotion is controlled by applying a static electric field to push the ions [22] along $\hat{x}$, moving ion 2 (ion 1) away from (toward) the rf null position, inducing a smaller (larger) Rabi frequency. The range of Rabi frequencies explored experimentally is shown in Fig. 2a.

We determine $\Omega_{1,2}$ by observing the Rabi oscillations of the ions (between $|\downarrow\rangle$ and $|\uparrow\rangle$) driven on the $\hat{x}$ carrier. An example with $\Omega_1 = 2\Omega_2$ is shown in Fig. 2b. We

FIG. 2. (a) Normalized $\hat{x}$-carrier Rabi frequencies Ω_i/Ω_c of each of two ions as a function of center-of-mass displacement d from the rf-null position. The solid curves are Eq. (3) where the distance between the maxima of the two curves sets the scale of the ordinate, based on the known ion-ion spacing of $l \approx 2.2$ μm at $\omega_x/2\pi = 8.8$ MHz. (b) Example of Rabi oscillations starting from the initial state $|\downarrow\downarrow\rangle|n = 0\rangle$ with $\Omega_1 = 2\Omega_2$. A fit to Eq. (4) determines that $\Omega_1/2\pi = 2\Omega_2/2\pi \approx 225$ kHz, $\gamma/2\pi \approx 6$ kHz, and $\alpha \approx -0.05$. The arrow in (a) indicates the conditions of (b).

detect a fluorescence signal $S(t) = 2P_{\downarrow\downarrow} + (1 + \alpha)P_{\downarrow\uparrow} + (1 - \alpha)P_{\uparrow\downarrow}$ where $P_{kl} = |\langle\psi(t)|kl\rangle|^2$, $k, l \in \{\uparrow, \downarrow\}$, $\psi(t)$ is the state at time t and $|\alpha| \ll 1$ describes a small differential detection efficiency due to the induced differential micromotion. Driving on the $\hat{x}$ carrier for time t starting from $|\downarrow\downarrow\rangle|0\rangle$, $S(t)$ can be described by

$$S(t) = 1 + (1/2)(1 + \alpha)\cos(2\Omega_1 t)e^{-\gamma t}$$
$$+ (1/2)(1 - \alpha)\cos(2\Omega_2 t)e^{-(\Omega_2/\Omega_1)\gamma t}, \quad (4)$$

where γ allows for decay of the signal [20]. The local maximum at $t = 2.4$ μs on Fig. 2b is the $2\pi{:}\pi$ point at which ion 1 has undergone a 2π pulse while ion 2 has undergone a π pulse resulting in $|\downarrow\downarrow\rangle|0\rangle \rightarrow |\downarrow\uparrow\rangle|0\rangle$. Driving a $\pi{:}\pi$ pulse on the copropagating carrier transforms $|\downarrow\uparrow\rangle|0\rangle$ to $|\uparrow\downarrow\rangle|0\rangle$ and $|\downarrow\downarrow\rangle|0\rangle$ to $|\uparrow\uparrow\rangle|0\rangle$, completing the generation of all four internal basis states of Fig. 1b.

Now consider the levels coupled by the first rsb [20] shown in Fig. 1b. If we start in the state $|\psi(0)\rangle = |\downarrow\uparrow\rangle|0\rangle$ and drive on the (stretch mode) rsb for time t, the Schrödinger equation can be integrated to yield

$$|\psi(t)\rangle = -\frac{i\Omega_{2-}}{G}\sin(Gt)|\downarrow\downarrow\rangle|1\rangle$$
$$+ \left[\frac{\Omega_{2-}^2}{G^2}(\cos Gt - 1) + 1\right]|\downarrow\uparrow\rangle|0\rangle$$
$$+ e^{i\phi}\left[\frac{\Omega_{2-}\Omega_{1-}}{G^2}(\cos Gt - 1)\right]|\uparrow\downarrow\rangle|0\rangle, \quad (5)$$

where $G = (\Omega_{2-}^2 + \Omega_{1-}^2)^{1/2}$ and Ω_{i-} is from Eq. (2) with $n = 0$. The phase factor $\phi = \delta\vec{k} \cdot \langle\vec{x}_1 - \vec{x}_2\rangle$ depends on the spatial separation of ions and the arises because each ion sees different laser phases. The ion-ion spacing varies by $\delta l \approx 100$ nm over the range of U_0 cited previously ($\phi = 0$ for $U_0 = 16.3$ V and $\phi = \pi$ for $U_0 = 12.6$ V, with $d\phi/dU_0$ in good agreement with theory). For $Gt = \pi$ and $\Omega_1 = 2\Omega_2$, the final state is $\psi_e(\phi)$ from Eq. (1). Note that $\Omega_1 = (\sqrt{2} + 1)\Omega_2$ would generate the Bell states (but we would not have access to the initial state $|\downarrow\uparrow\rangle$, since Ω_i are fixed throughout an experiment).

We now describe our two-ion state-detection procedure. We first prepare a two-ion basis state $|kl\rangle$, apply the detection beam D2 for a time $\tau_d \approx 500$ μs, and record the number of photons m detected in time τ_d. We repeat this sequence for $N \approx 10^4$ trials and build a histogram of the photons collected (Fig. 3). To determine the population of an unknown state, we fit its histogram to a weighted sum of the four basis histograms with a simple linear least-squares procedure.

We observe that the $|\uparrow\uparrow\rangle$ count distribution (Fig. 3a) is not the expected single peak at $m = 0$, but includes contributions at $m = 1$ and $m = 2$ due to background counts. The signal in bins $m > 2$ (which accounts for ~10% of the area) is due to a depumping process in which
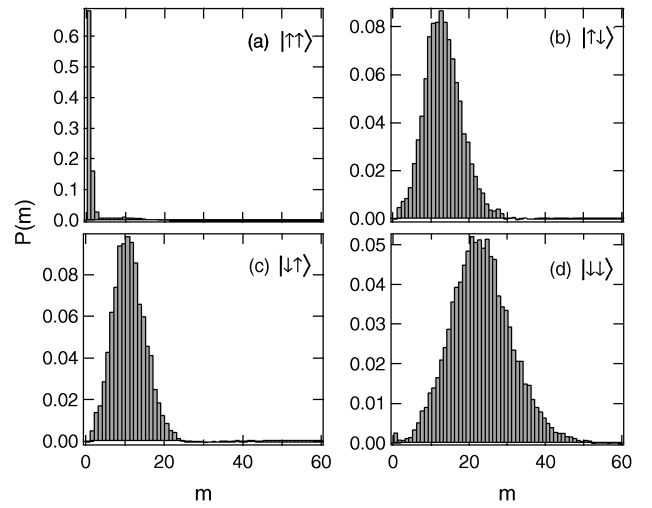

FIG. 3. Photon-number distributions for the four basis qubit states. Plotted in each graph is the probability of occurrence $P(m)$ of m photons detected in 500 μs vs m, taken over ~10^4 trials. Note the different scales for each graph.

D2 off-resonantly drives an ion out of $|\uparrow\rangle$, ultimately trapping it in the cycling transition. We approximately double the depumping time by applying two additional Raman "shelving" pulses ($|\uparrow\rangle \rightarrow ^2S_{1/2}|F = 2, m_F = 0\rangle \rightarrow ^2S_{1/2}|F = 1, m_F = -1\rangle$; $|\downarrow\rangle$ unaffected) after every state preparation. This results in an average difference of 10–15 detected photons between an initial $|\downarrow\rangle$ and $|\uparrow\rangle$ state, as shown in Fig. 3. The distributions associated with $|\downarrow\uparrow\rangle$, $|\uparrow\downarrow\rangle$, and $|\downarrow\downarrow\rangle$ are non-Poissonian due to detection laser intensity and frequency fluctuations, the depumping described previously and $|\downarrow\rangle \rightarrow |\uparrow\rangle$ transitions from imperfect polarization of D2.

One may ask: What is our overall two-ion state-detection efficiency on a *per experiment* basis? To address this issue, we distinguish three cases: (1) $|\uparrow\uparrow\rangle$, (2) $|\uparrow\downarrow\rangle$ or $|\downarrow\uparrow\rangle$, and (3) $|\downarrow\downarrow\rangle$. Now define case 1 to be true when $m \leq 3$, case 2 when $3 < m < 17$, and case 3 when $m \geq 17$. This gives an optimal 80% probability that the correct case is diagnosed.

We have generated states described by density operators $\rho^{\pm}$ in which the populations (diagonals of $\rho^{\pm}$) are measured to be $P_{\downarrow\uparrow} \approx P_{\uparrow\downarrow} \approx 0.4$, $P_{\downarrow\downarrow} \approx 0.15$, and $P_{\uparrow\uparrow} \approx 0.05$. To establish coherence, consider first the Bell singlet state ψ_B^- which has $P_{\downarrow\uparrow} = P_{\uparrow\downarrow} = 1/2$. Since ψ_B^- has total spin $J = 0$, any J-preserving transformation, such as an equal rotation on both spins, must leave this state unchanged, whereas such a rotation on a mixed state with populations $P_{\downarrow\uparrow} = P_{\uparrow\downarrow} = 1/2$ and no coherences will evolve quite differently. We perform a rotation on both spins through an angle θ by driving on the copropagating carrier for a time t such that $\theta = \Omega_c t$. Figure 4a shows the time evolution of an experimental state which approximates the singlet Bell state. Contrast this with the approximate "triplet" state shown in Fig. 4b. The data show that $\rho^{\pm}$ is decomposed as $\rho^{\pm} = C|\psi_B^{\pm}\rangle\langle\psi_B^{\pm}| + (1 - C)\rho_m$
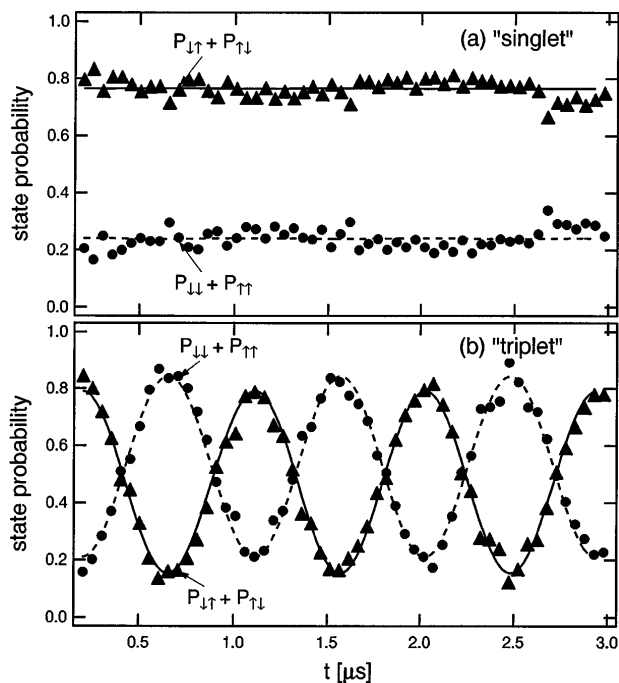
FIG. 4.   Probabilities $P_{\uparrow\uparrow} + P_{\uparrow\downarrow}$ and $P_{\downarrow\downarrow} + P_{\uparrow\uparrow}$ as a function of time t driving on the copropagating carrier, starting from (a) the "singlet" $\psi_e(0)$ and (b) the "triplet" $\psi_e(\pi)$ entangled states. The equivalent rotation angle is $2\Omega_c t$ ($\Omega_c/2\pi \approx 200$ kHz for these data). The solid and dashed lines in (a) and (b) are sinusoidal fits to the data, from which the contrast is extracted.

in which ρ_m has no coherences which contribute to the measured signal (off-diagonal elements connecting $|\uparrow\downarrow\rangle$ with $|\downarrow\uparrow\rangle$ and $|\uparrow\uparrow\rangle$ with $|\downarrow\downarrow\rangle$), and $C = 0.6$ is the contrast of the curves in Fig. 4. This leads to a fidelity of $\langle \psi_B^\pm | \rho^\pm | \psi_B^\pm \rangle = (P_{\uparrow\downarrow} + P_{\uparrow\downarrow} + C)/2 \approx 0.7$.

The nonunit fidelity of our states arises from Raman laser intensity noise and a second-order (in η) effect on Ω_i due to excitation of the c.m. mode [19]. These effects can be seen in Fig. 2b as a decay envelope on the data [modeled by γ of Eq. (4)] and cause a 10% loss of fidelity in initial state preparation [23].

The micromotion-induced selection of Rabi frequencies as here demonstrated is sufficient to implement two-ion universal quantum logic with individual addressing [8]. To start, we arrange the trap strength and static electric field in such a way that $|\delta\vec{k}|\xi_1 = 0$ and $|\delta\vec{k}|\xi_2 = a_0$, where $J_0(a_0) = 0$. To isolate ion 1, note that by Eq. (3) $\Omega_1 = \Omega_c J_0(0) = \Omega_c$ and $\Omega_2 = \Omega_c J_0(a_0) = 0$. To isolate ion 2, we add $\Omega_T/2\pi = \pm 238$ MHz to the difference frequency of the Raman beams. This drives the first sideband of the rf micromotion so that the J_0 of Eq. (3) is replaced by J_1, resulting in $\Omega_1 = \Omega_c J_1(0) = 0$ and $\Omega_2 = \Omega_c J_1(a_0) \neq 0$.

In conclusion, we have taken a first step which is crucial for quantum computations with trapped ions. We have *engineered* entangled states deterministically; that is, there is no inherent probabilistic nature to our quantum entangling source. We have developed a two-ion state-sensitive detection technique which allows us to measure the diagonal elements of the density matrix $\rho^\pm$ of our states, and have performed transformations which directly measure the relevant off-diagonal coherences of $\rho^\pm$.

*Electronic address: quentint@boulder.nist.gov.
†Present address: Univ. Innsbruck, Innsbruck, Austria.

 [1] A. Einstein, B. Podolsky, and N. Rosen, Phys. Rev. **47**, 777 (1935); J.S. Bell, *Speakable and Unspeakable in Quantum Mechanics* (Cambridge University Press, Cambridge, England, 1987).
 [2] P.W. Shor, SIAM J. Comput. **26**, 1484 (1997); L.K. Grover, Phys. Rev. Lett. **79**, 325 (1997).
 [3] A. Barenco and A. Ekert, J. Mod. Opt. **42**, 1253 (1995); C.H. Bennett, Phys. Today **48**, No. 10, 24 (1995).
 [4] A. Ekert, Phys. Rev. Lett. **67**, 661 (1991); C.H. Bennett, Sci. Am. **267**, No. 4, 50 (1992).
 [5] J.J. Bollinger *et al.,* Phys. Rev. A **54**, R4649 (1996); S.F. Huelga *et al.,* Phys. Rev. Lett. **79**, 3865 (1997).
 [6] D.J. Wineland *et al.,* J. Res. Natl. Inst. Stand. Technol. **103**, 259 (1998).
 [7] A. Ekert and R. Jozsa, Rev. Mod. Phys. **68**, 733 (1996); A. Steane, Rep. Prog. Phys. **61**, 117 (1998).
 [8] J.I. Cirac and P. Zoller, Phys. Rev. Lett. **74**, 4091 (1995).
 [9] C. Monroe *et al.,* Phys. Rev. Lett. **75**, 4714 (1995).
[10] S.J. Freedman and J.F. Clauser, Phys. Rev. Lett. **28**, 938 (1972); E.S. Fry and R.C. Thompson, Phys. Rev. Lett. **37**, 465 (1976); A. Aspect, P. Grangier, and G. Roger, Phys. Rev. Lett. **49**, 91 (1982).
[11] Z.Y. Ou and L. Mandel, Phys. Rev. Lett. **61**, 50 (1988); Y.H. Shih and C.O. Alley, Phys. Rev. Lett. **68**, 3663 (1992); Z.Y. Ou *et al.,* Phys. Rev. Lett. **68**, 3663 (1992); P. Kwiat *et al.,* Phys. Rev. Lett. **75**, 4337 (1995); W. Tittel *et al.,* Europhys. Lett. **40**, 595 (1997); D. Bouwmeester *et al.,* Nature (London) **390**, 575 (1997).
[12] M. Lamehi-Rachti and W. Mittig, Phys. Rev. D **14**, 2543 (1976).
[13] E. Hagley *et al.,* Phys. Rev. Lett. **79**, 1 (1997).
[14] R. Laflamme *et al.,* quant-ph/9709025 (unpublished).
[15] I.L. Chuang, N. Gershenfeld, and M. Kubinec, Phys. Rev. Lett. **80**, 3408 (1998); I.L. Chuang *et al.,* Nature (London) **393**, 143 (1998); D.G. Cory, M.D. Price, and T.F. Havel, Physica (Amsterdam) **120D**, 82 (1998); D.G. Cory *et al.,* Phys. Rev. Lett. **81**, 2152 (1998).
[16] C.K. Law and H.J. Kimble, J. Mod. Opt. **44**, 2067 (1997).
[17] J.I. Cirac *et al.,* Phys. Rev. Lett. **78**, 3221 (1997).
[18] C.H. Bennett *et al.,* Phys. Rev. A **53**, 2046 (1996).
[19] B.E. King *et al.,* Phys. Rev. Lett. **81**, 1525 (1998).
[20] D.M. Meekhof *et al.,* Phys. Rev. Lett. **76**, 1796 (1996); **77**, 2346 (1996).
[21] D.J. Wineland and W.M. Itano, Phys. Rev. A **20**, 1521 (1979).
[22] S.R. Jefferts *et al.,* Phys. Rev. A **51**, 3112 (1995).
[23] The reference histograms for $|\downarrow\downarrow\rangle$ and $|\uparrow\downarrow\rangle$ (Figs. 3b and 3c) have had this 10% contamination from $|\uparrow\uparrow\rangle$ and $|\downarrow\downarrow\rangle$ removed.